Fluorescence Imaging of Electrical Activity in Cardiac Cells Using An All-Solid-State System

Emilia Entcheva*, *Member, IEEE*, Yordan Kostov, *Member, IEEE*, Elko Tchernev, and Leslie Tung, *Member, IEEE*

***Abstract*—Tracking spatial and temporal determinants of cardiac arrhythmogenesis at the cellular level presents challenges to the optical mapping techniques employed. In this paper, we describe a compact system combining two nontraditional low-cost solutions for excitation light sources and emission filters in fluorescence measurements of transmembrane potentials, V_m, or intracellular calcium, $[Ca^{2+}]_i$ in cardiac cell networks. This is the first reported use of high-power blue and green light emitting diodes (LEDs), to excite cell monolayers stained with V_m - (di-8-ANEPPS) or $[Ca^{2+}]_i$ – (Fluo-3) sensitive dyes. In addition, we use simple techniques for fabrication of suitable thin emission filters with uniform properties, no auto-fluorescence, high durability and good flexibility for imaging V_m or $[Ca^{2+}]_i$. The battery-operated LEDs and the fabricated emission filters, integrated with a fiber-optic system for contact fluorescence imaging, were used as tools to characterize conduction velocity restitution at the macro-scale. The versatility of the LEDs for illumination is further emphasized through 1) demonstration of their usage for epi-illumination recordings at the single-cell level, and 2) demonstration of their unique high-frequency light modulation ability. The LEDs showed excellent stability as excitation light sources for fluorescence measurements; acceptable signal-to-noise ratio and negligible cell photodamage and indicator dye photobleaching were observed.**

***Index Terms*—Calcium, cultured cardiac cells, LED excitation, optical mapping, voltage-sensitive dyes.**

I. Introduction

OPTICAL mapping using voltage- and calcium-sensitive dyes has become a major experimental tool to study cardiac electrical activity [1], [2] due to its superior spatiotemporal performance over more traditional mapping methods. Two approaches have been employed in the design of such systems: broad illumination of the target with multiple photodetectors [charge-coupled devices (CCDs) or photodiode arrays] or spot illumination and raster scanning of the target with a single photodetector (laser scanning methods). Successful applications of these include optical mapping in isolated tissue preparations and whole heart [3]–[7].

Recently, a new experimental multicellular preparation has emerged in the studies of cardiac electrical activity. The use of confluent monolayers and patterned growth of cultured mammalian cardiac cells [8] offers an attractive alternative to tissue studies in basic cardiac research. Although microscopic optical mapping has proven to be an invaluable tool for revealing subtle details about impulse propagation in and electrical stimulation of cardiac cell networks [9]–[11] there are drawbacks that render it unsuitable for studies of phenomena requiring macroscopic, long-term monitoring. The main disadvantage is the limited field of view. In addition, collection of fluorescent signals from a very small area requires high intensity of the excitation light, which leads to high levels of phototoxic cell damage [12] and fluorescent dye bleaching over short exposure times. Two recent studies report macroscopic long-term optical imaging of reentrant activity in monolayers of cultured cardiac cells: 1) measurements of intracellular calcium waves using a CCD camera and calcium-sensitive dye Fluo-3 [13]; and 2) contact fluorescence imaging (CFI) of transmembrane potentials using voltage-sensitive dye di-8-ANEPPS [14]. The latter optical imaging technique was developed in our laboratory, and is extended in this paper. CFI is a fiber-optic approach that takes advantage of the planar nature of the cell culture monolayer grown on a transparent thin carrier, thus making imaging possible without relay lenses between the optical fiber bundle and the coverslip.

The progress in optical mapping of excitable tissue has been facilitated by the development of faster and more sensitive photodetectors [5], [10], [15] the development of better fluorescent probes [16], and their combined use [9]. This paper puts the emphasis on the selection of illuminators and filters as an important part of the fluorescence measurement. The goal was to design enhanced, cost-effective modules for CFI (but also applicable in all optical mapping systems of cardiac electrical activity), including the use of: 1) solid-state excitation light sources [high power light emitting diodes (LEDs)] and 2) wavelength selection through plastic low-cost filters. The versatility of the new illumination is demonstrated in macro- and micro-scale fluorescence measurements of transmembrane potentials or intracellular calcium in cardiac cells, detailing events at the single cell and the tissue level. Parts of this work have been presented in an abstract form [17].

Manuscript received October 30, 2002; revised June 8, 2003. The work of E. Entcheva was supported in part by the American Heart Association (Mid-Atlantic Affiliate) through Postdoctoral Fellowship 9920393U. The work of L. Tung was supported in part by the National Institutes of Health (NIH) under Grant HL48266 and Grant HL66239. *Asterisk indicates corresponding author.*

*E. Entcheva was with the Department of Biomedical Engineering, The Johns Hopkins University School of Medicine, Baltimore, MD 21250 USA. She is now with the Department of Biomedical Engineering, State University of New York at Stony Brook, HSC T18-030, Stony Brook, NY 11794-8181 USA (e-mail: email: emilia.entcheva@sunysb.edu).

Y. Kostov is with the Department of Chemical and Biochemical Engineering, University of Maryland – Baltimore County, Baltimore, MD 21250 USA.

E. Tchernev is with the Department of Computer Science, University of Maryland – Baltimore County, Baltimore, MD 21250 USA.

L. Tung is with the Department of Biomedical Engineering The Johns Hopkins University School of Medicine, Baltimore, MD 21205 USA.

Digital Object Identifier 10.1109/TBME.2003.820376

II. Materials and Methods

A. Experimental Preparation: Monolayers of Cultured Cardiac Cells

Confluent cell monolayers grown from neonatal rat cardiac myocytes were used for the experiments, as described previously [14]. Briefly, cells were isolated from the hearts (ventricles) of 3–4 day old Sprague-Dawley rats, trypsin dissociated and plated onto circular glass coverslips (22 mm, no. 1, VWR, Media, PA) that were precovered with a thin layer of collagen, laminin or fibronectin. Cells were then cultured for 4–6 days in a 5% CO_2 incubator at 37 °C and maintained by replacement of culture medium.

During experiments, the coverslips were transferred to a custom made experimental chamber, and the cells were superfused with normal Tyrode's solution (in mM): 135 NaCl, 5.4 KCl, 1.8 $CaCl_2$, 1 $MgCl_2$, 0.33 NaH_2PO_4, 5 HEPES, 5 glucose, adjusted to pH 7.4 with NaOH. Experiments were conducted at elevated temperature (33 °C–35 °C) and 1.3 mM extracellular $[Ca^{2+}]$.

For transmembrane potential measurements, the cell monolayers were incubated with 75–100 μM of the voltage-sensitive dye di-8-ANEPPS (Molecular Probes, Eugene, OR) for 5 min. For the intracellular calcium ($[Ca^{2+}]_i$) measurements, we stained the cells with Fluo-3-AM (Molecular Probes) by adding 1 ml 15 μM dye solution to the still wet experimental chamber. The loading time (at room temperature) was 30 min for the AM form of the dye to enter the cells through passive diffusion and an additional 30 min (after washing the excess dye) for the cell esterases to cleave off the AM segment of the indicator.

B. Measurement and Data Acquisition System

Macro-scale measurements were performed using CFI. Briefly, excitation light was delivered at an angle from the top of the coverslip (via transillumination). The emitted fluorescent signals were filtered through a thin emission filter covering the bottom side of the coverslip and collected by an optical fiber bundle array (plastic optical fibers 1 mm diameter, NA 0.5, Boston Optical, Westborough, MA). The front ends of the fibers were epoxied together using hexagonal packing, and polished with a perpendicular flat surface. The front end was pushed up against the emission filter and formed a plane parallel to the coverslip. The free back ends of the fibers were coupled to individual photodetectors (S6786, Hamamatsu) and the optical mapping instrumentation system. After amplification (trans-impedance amplifier with a 100 MΩ feedback resistor, and additional 20 × amplification, distributed in two stages [14]), the signals were digitized (data acquisition board, 16 bit ADC, SI-DSP6400–200, Sheldon Instruments, Provo, UT) and stored for further analysis. The sampling rate was set via data acquisition software (LabVIEW, National Instruments, Austin, TX) at 1000 samples per second per channel. The acquired signals were filtered, if necessary, using a temporal median filter (sliding window size 3 to 11 sample points). This type of filter is a natural choice (and is widely used), since it preserves step changes, such as the action potential upstroke, and does not introduce phase shifts, as shown previously [18].

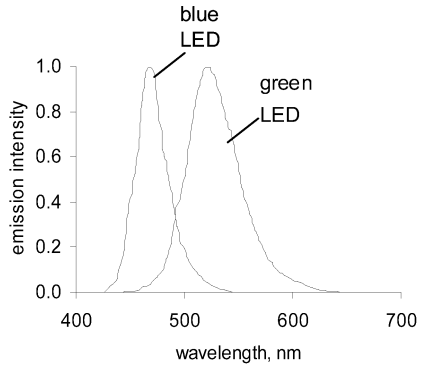

Fig. 1. Relative emission intensity spectra for the blue (NSPB500S, Nichia) and green (NSPG500S, Nichia) high-power LEDs used in the system.

Microscopic measurements were performed using a Nikon Eclipse TS100 microscope, with a 20 × S Fluor objective (N.A. 0.75). Excitation light was delivered through epi-illumination and emitted fluorescence was collected using a photomultiplier tube (PMT, Electron Tubes Lmtd, UK) with a band-pass filter 610/75 nm (Omega Optical, Brattleboro, VT). Sampling rate and data analysis were the same as in the macro-measurements.

C. Solid-State Excitation Light Sources

1) Requirements for the Excitation Light Sources: Traditional light sources to excite fluorescent indicators in live cells include: high-pressure xenon (Xe) arc lamps, high-pressure mercury (Hg) lamps, mercury-xenon (Hg-Xe) arc lamps, and quartz-tungsten halogen (QTH) lamps [19]. All of the above, except the Hg lamps, output stable high-power light and have a continuous spectrum covering the desired range (400–700 nm). Semiconductor-generated illumination is an attractive alternative, although the limited output power of these otherwise compact, inexpensive, and very versatile light sources has prevented their use in fluorescence imaging. Several technological innovations (involving gallium nitride (GaN) compounds) have recently allowed the mass production of high-power LEDs and laser diodes over a wide range of wavelengths, including those of interest for fluorescence measurements in living cells.

2) LED Characteristics: Fig. 1 illustrates the manufacturer-supplied emission spectra (relative intensity) for the green (NSPG500S, Nichia America, Mountville, PA) and blue (NSPB500S, Nichia) high-power LEDs selected for this study. The intensity maxima are consistent with the excitation spectra for di-8-ANEPPS and Fluo-3 [20], [21] respectively. The intensity output is typically 10 candela (cd) (maximum 17 cd) for the green LEDs and 3.6 cd (maximum 7.2 cd) for the blue LEDs. The manufacturer (Nichia) supplies information only in candela (linked to the human eye photosensitivity). The conversion from candela into Watts [22] for comparison to other light sources can be done after some considerations and assumptions, and yields about 1.7 (5.5) mW and 3(11) mW for the typical (maximum) optical power of the green and the blue LED, respectively. Actual measurements of optical power are reported in the Section III.

3) Block Diagram: In this paper, the LEDs were used in a constant current (60 mA) continuous illumination mode. The block diagram is shown in Fig. 2(a). We use a 9.6 V recharge-

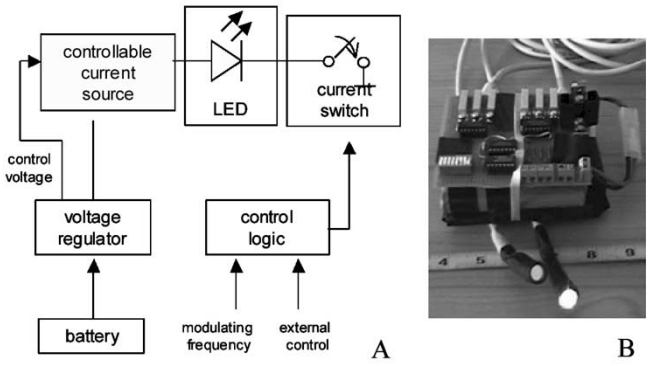

Fig. 2. Illumination module with semiconductor light sources (LEDs). **A** Block diagram. The battery is a Radio Shack 9.6 V race-car battery. Voltage regulators (TL7806) maintain $+6$ V. The controllable current source for each LED is transistor-based (2N2907A). The current switches include open-collector integrated circuits (74LS06) and additional logic for external control signals (TTL levels) to enable/disable illumination. **B** Photograph of the illumination module.

able nickel-metal hydride battery and voltage regulators to supply $+6$ V (TL7806). The controllable current source for each LED was transistor-based (PNP transistor 2N2907A). The control switchboard consisted of open-collector current switches (74LS06) and additional logic for computer-generated external control signals (TTL levels) to enable/disable illumination. All components were purchased from Radio Shack (Fort Worth, TX). A photograph of the actual illumination module is shown in Fig. 2(b).

During macroscopic measurements, the LED unit was fixed with a clamp at a permanent position, forming about 45 degrees with the plane of the experimental chamber, 15 mm from the sample on the upper side, similar to the liquid light guide, used in measurements with a QTH lamp. After experimenting, this position was found to work well in illuminating the sample and minimizing the coupling of the excitation light into the light-collecting optical fibers (NA 0.5). For microscopic measurements, the LED module was coupled to the standard epi-illumination attachment of the microscope, assuring uniform light at the back focal plane of the objective.

4) Stability Assessment: To assess the stability of the LEDs and the 250-W QTH lamp (Oriel, Stratford Connecticut) as light sources, we measured the output of a blue and green LED and the lamp over 10 min of continuous illumination, with 1 kHz sampling frequency. The noise of the light sources was compared after normalization to the signal amplitude. Fourier analysis was done in Matlab using the Welch's method (1024 points) with a Hamming window for estimating the power spectrum density (PSD) in the interval 0–500 Hz.

D. Emission Filters for Macroscopic Measurements

1) Requirements for the Emission Filters: Optical emission filters must have good absorbance properties for the wavelengths to be suppressed (excitation light range) and good transmittance for the emitted fluorescent light from the sample. Additional requirements include a lack of auto-fluorescence, as well as a good durability in terms of easy handling, long shelf life, and resistance to physiological solutions. The lack of a focal plane in CFI (no relay lenses are used between the sample and the photodetectors) imposes one more requirement—the thickness of the emission filter must be small compared with the spacing between adjacent channels (1 or 2 mm in our system). This is needed to avoid crosstalk between channels as the separation distance between the sample and the fiber bundle increases (theoretically and experimentally assessed in our previous study [14]). An alternative placement for the filters in CFI would be directly in front of the photodetectors. However, such a solution is 1) cumbersome and expensive, requiring N individual filters for the N channels; and 2) does not resolve the thickness issue, since to collect all the light from an optical fiber (NA 0.5) through a thick emission filter requires a large-area photodetector, which leads to undesirable increase in the capacitance noise. The standard commercially available optical filters are on the order of 1 mm or more. The Kodak gelatin WRATTEN filters (Eastman Kodak Co., Rochester, NY) are one exception, with a thickness of only 100 μm and potentially suitable spectral characteristics. However, our experiments with them revealed significant auto-fluorescence in the range of the emission wavelengths, and the lack of tolerance to any exposure to solutions (a severe handicap for physiological experiments). Therefore, we explored alternative approaches for custom-designing thin filters, appropriate for CFI.

2) Preparation Procedures: The following simple recipes for dye entrapment were used to obtain emission membrane filters. For the calcium filters a mixture containing 1 g cellulose acetate (Aldrich Chemical, Milwaukee, WI), 0.5 ml triethyl citrate (Aldrich) and 17 ml of spectroscopic grade acetone (Adrich) was prepared and left in a covered jar overnight to obtain a clear solution. Then a dye solution was made—$2\ \mathrm{mg/ml}$ Acid Yellow 99 (Aldrich) in 1 ml of methyl alcohol (Aldrich) and 2 ml of acetone—and added to the cellulose mixture. Three to four ml of solution were poured into 60-mm glass Petri dishes and allowed to dry slowly (covered overnight) to form thin (50–200 μm) membranes with uniform properties, no auto-fluorescence and good flexibility and durability.

The cellulose acetate matrix was found to be unsuitable for preparing filters for transmembrane potential measurements due to low solubility of the selected dyes in it. Two kinds of red emission filters (for $\mathrm{V_m}$) were made using alternative carriers. In the first approach, Congo Red (Aldrich) was dissolved in water to form a saturated solution (1 mg/ml). A separate mixture was prepared using equal parts of acetone (Aldrich) and a Quick Set Epoxy (Loctite Corp., Rocky Hill, CT) containing epoxy resin and amine-based epoxy hardener. The epoxy solution was poured onto a microscope glass slide to form a layer of 150 μm thickness. After drying for 24 h, the glass slide with the transparent solid epoxy layer (about 60–120 μm thick) was soaked in the Congo Red solution overnight. The obtained emission filters, entrapping the red dye, were readily detachable from the glass carrier.

The second technique for $\mathrm{V_m}$ filters involved red ink extracted from an Avery–Dennison marker (Mt. Prospect, IL) that was incorporated into a layer of silicone elastomer. Approximately 15 mg of the two components of a Sylgard 184 kit (Dow Corning, Midland, MI) were mixed in the usual 1:10 ratio; 0.5 ml of ink extract was stirred in and the mixture was poured in 10-mm plastic Petri dishes. After removal of all air bubbles,

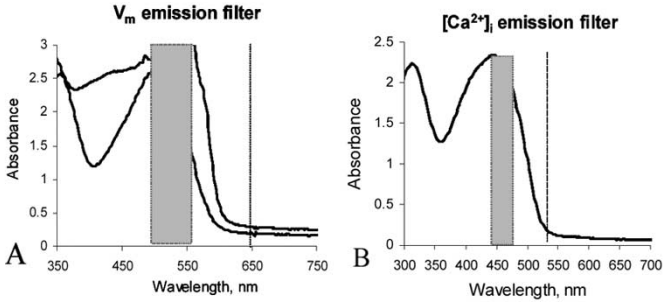

Fig. 3. Absorption spectra of the membrane emission filters: **A** for $\mathrm{V_m}$ measurements with a Congo Red epoxy membrane and with a red ink silicone membrane (spectrum shifted to the right); and **B** for $[\mathrm{Ca}^{2+}]_\mathrm{i}$ measurements with Acid Yellow 99. The wavelength band for the delivered excitation light (to be absorbed by the filter) and the peak wavelength for the emitted fluorescent light (to be transmitted by the filter) are indicated with the shaded region and the dotted line, respectively.

the mixture was baked for 2 h at 60 °C, and the cured silicone membranes were easily removed and ready to use. Because of limited ink entrapment, this approach was only used to fabricate membranes thicker than 400 μm, suitable for recordings with a larger spacing (2 mm) between the detecting optical fibers.

III. Results

A. System Description

The illumination modules were designed with a minimum number of three parallel green LEDs with a common interference excitation filter (bandpass 525 ± 35 nm, Intor, Socorro, NM) for $\mathrm{V_m}$ and with three blue LEDs with a common excitation filter (bandpass 460 ± 15 nm, Intor) for $[\mathrm{Ca}^{2+}]_\mathrm{i}$. The output optical power for the green LED module was 6.1 $\mathrm{mW/cm^2}$ and for the blue LED module was 5.4 $\mathrm{mW/cm^2}$, as determined by an optical power meter (Model 849-C, Newport). The cost per excitation light module (three LEDs, electronics, power supply, filter and cables) was at least an order of magnitude less than the traditional lamps currently in use.

The dyes (Acid Yellow 99, Congo Red and the red marker ink) for the emission filters were selected after screening about a dozen dyes with potentially suitable spectral characteristics and no auto-fluorescence. The matrix and the dye concentration were chosen after trial and error for best membrane properties. The flexibility and durability of the yellow membranes were adjusted by the ratio of cellulose acetate and triethyl citrate used; without triethyl citrate, the fabricated membranes were very brittle and difficult to handle.

The spectral characteristics of the fabricated emission filters are shown in Fig. 3. Suppression of 2–3 orders of magnitude ($\mathrm{absorbance} > 2.5$) was attained in the range of the excitation light wavelengths. The silicone membrane with red ink had a more suitable spectral profile (a steeper slope and a greater absorbance in the overlap region between the excitation and emission wavelengths) compared to the Congo Red epoxy membrane. All membranes had $\mathrm{transmittance} > 50\%$ at the peak emission wavelengths (peak emission at 526 nm for Fluo-3; and at 650 nm for di-8-ANEPPS [21]). The Congo Red membrane characterized in Fig. 3(a) was 95 μm thick, the red ink silicone membrane in Fig. 3(a) was 550 μm thick and the Acid Yellow 99 membrane in Fig. 3(b) was 80 μm thick. The output fluorescence of all manufactured filters was indistinguishable from the noise level in measurements at high amplification with a Perkin-Elmer fluorimeter MPF 66. In comparison, the fluorescence of the WRATTEN filters was several orders of magnitude higher, visible by eye. According to the Beer–Lambert law [19], absorption of the excitation light is linearly proportional to the thickness and the dye concentration in the membrane. Thus, by regulating the latter two parameters, some flexibility exists to control the emission filter properties.

The fabricated emission filters were positioned immediately underneath the glass coverslips on top of the imaging optical fiber bundle in the CFI system, and used for $\mathrm{V_m}$ and $[\mathrm{Ca}]_\mathrm{i}$ macroscopic recordings in cultured monolayers of neonatal rat ventricular myocytes. They were not in direct contact with the cells at any point. However, the coverslips formed the bottom of the experimental chamber; thus during mounting/dismounting or during perfusion while experimenting, it was possible to get solution on the filters. The filters were reusable and could tolerate long exposure to water-based solutions. No dye came out in solution, and the membrane properties remained unchanged after a week of soaking.

B. Excitation Light Source Stability

No specific frequency peaks were introduced by either light source (LEDs or lamp): the power spectrum density was uniformly elevated across the frequencies 7–500 Hz compared to the corresponding values for a detector in dark; noise levels for frequencies in the 0–7 Hz range were significantly higher. Overall the blue LED had the lowest noise, and the QTH lamp had the highest level of noise. In the frequency range 7–500 Hz, the green LED and the lamp had respectively 6 dB and 8.6 dB higher noise than the blue LED. In the low-frequency range (0–7 Hz), the blue LED still performed better than the other light sources: the lamp introduced 21 dB more noise, and the green LED had 9 dB higher noise than the blue LED. A decibel (dB) is the usual measure for noise related to a 1-V signal at a given frequency; i.e., $10 \log (P(\mathrm{noise})/P(1\ \mathrm{Vsignal}))$ where P represents power.

The baseline low-frequency changes were monotonic (linear) for the LEDs, and oscillatory for the lamp. Baseline change within 10 min continuous illumination was less than 4.9% (max deviation after binning in seconds) for the QTH lamp, less than 0.4% for the green LED, and less than 0.15% for the blue LED. In summary, for the examined frequency range (0–500 Hz), the LEDs showed better stability and lower noise than the QTH lamp used, with the blue LED – consistently performing best.

C. Macroscopic Imaging of Transmembrane Potentials

Fig. 4 demonstrates the quality of the macroscopic (CFI) transmembrane potential recordings for a confluent monolayer of cells, stained with voltage-sensitive dye. In the experiment presented in Fig. 4(a) and (b), cells were field stimulated at 1 Hz. 36 recording channels were arranged in a hexagonal pattern, with each spatial element 1 mm in diameter. The traces have been filtered (5-point median filter) and normalized to the

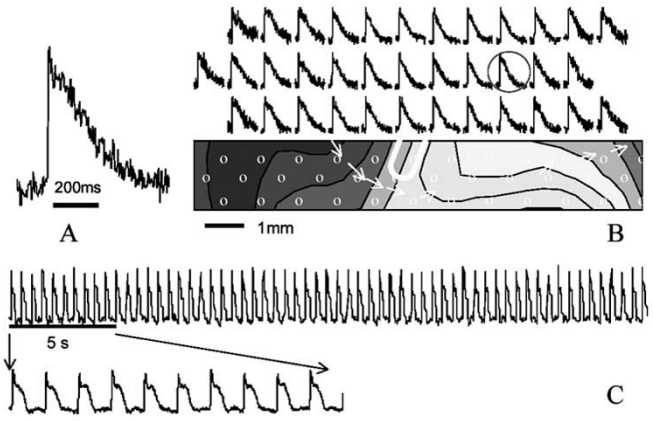

Fig. 4. V_m fluorescence signals. **A** Single channel recording is presented as normalized fluorescence, pacing at 1 Hz. **B** V_m multisite recordings, 36 channels arranged hexagonally in 3 rows –12 channels each, same experiment as in **A**. The corresponding isochrone-based activation map (propagation left-to-right, isochrones are 2 ms apart) shows a slow conduction region in the middle of the field of view. **C** Long 30 s recording (with the first 5 s given at a larger scale) from a different experiment, after multiple exposures shows the relative stability of the base line, pacing at 2 Hz.

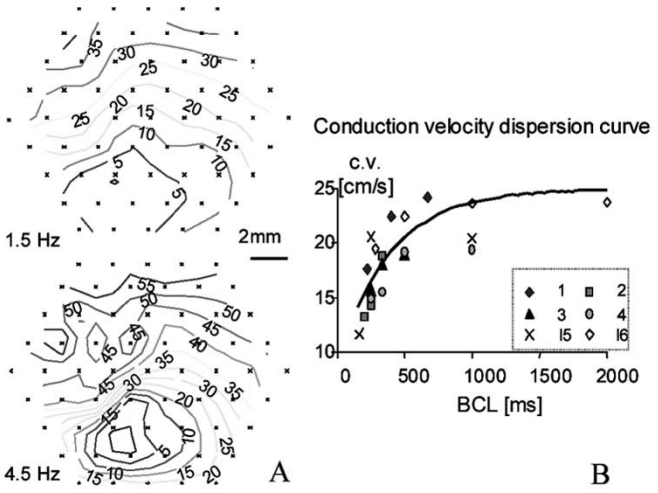

Fig. 5. Conduction velocity, CV, dispersion properties measured through macroscopic V_m recordings. **A** Activation maps (isochrones 5 ms apart) for point stimulation at 1.5- and 4.5-Hz pacing frequency. Maps were constructed from V_m measurements with 61 hexagonally spaced channels, 2 mm apart along the x-axis, covering an approximate circular area 16 mm in diameter. **B** Combined conduction velocity data [cm/s] for 6 monolayers (different symbols used), stimulated at different BCLs. Two of the six samples (l5 and l6) represent data obtained under QTH lamp illumination; the rest – LED illumination. The equation used to fit all data points with RMSE = 11% is: $CV = 25 - 10.5 * \exp(-(BCL - 167/390))$.

maximum value. Based on the time of 50% upstroke [10] at each spatial point, an activation map was constructed. The propagation was from left to right (cathode-to-anode), and a slow conduction zone that disturbed the activation pattern was apparent in the middle of the field of view. Fig. 4(c) is from an experiment in a different monolayer using the same membrane. Action potential morphology appears different, with a more pronounced plateau phase, typical for cells in earlier days in culture. This long 30 s recording was taken after multiple light exposures and demonstrates the relative stability of the baseline. The change (elevation) in the baseline was 11% of the amplitude of the signal for the 30 s shown.

D. Characterization of Conduction Velocity Restitution

In Fig. 5, we characterize the dispersion in conduction velocity when the cardiac cell monolayers are paced (point stimulation) at different frequencies. Pacing at a given basic cycle length (BCL) was applied for 30–60 s before the measurement. LED illumination was used to obtain transmembrane potential recordings and to construct activation maps (at 50% action potential upstroke [10], [9]). Using the average magnitude of the inverse gradients of the activation times at the different recording sites, we obtained global estimates for the conduction velocity under different conditions. For example, the (mean $\pm$ standard deviation) conduction velocity at 1.5-Hz pacing in Fig. 5(a) was 24.2 ± 3.6 cm/s, while the global estimate for 4.5-Hz pacing dropped to 17.6 ± 7.1 cm/s. Conduction velocity data for 6 coverslips are summarized in Fig. 5(b). Two of the 6 data sets were obtained under 200-W QTH lamp illumination (bandpass excitation filter (Chroma Technology, Brattleboro, VT): 535 ± 25 nm), to illustrate that functional properties measured by the new illumination method are consistent with lamp-based measurements. After an iterative procedure to minimize the root-mean-squared error (RMSE), a fitting curve was obtained using all data points. This conduction velocity dispersion curve relates C.V. (y) and BCL (x) and is in the form $y = y_{\max} - b * \exp(-(x - x_{\min}/\tau))$. The parameters and

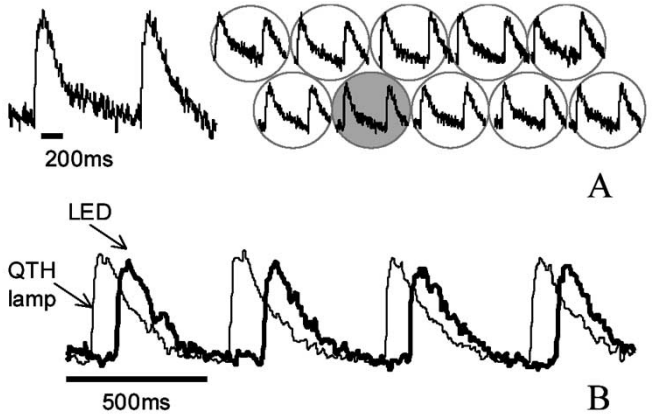

Fig. 6. Macroscopic $[Ca^{2+}]_i$ fluorescence signals. **A** Normalized single channel recording of $[Ca^{2+}]_i$; and spatial $[Ca^{2+}]_i$ signals (10 hexagonally arranged channels) from the same experiment. The single channel recording is indicated with a shaded circle. Cells were paced at 2 Hz. The Acid Yellow emission filter was the same as that characterized in Fig. 3(b). **B** $[Ca^{2+}]_i$ signals with the QTH lamp or the LED illumination module at the same spatial location, offset in time for clarity.

their empirically obtained values are as follows: $y_{\max}$ is the asymptotic C.V., $y_{\max} = 25$ (in cm/s); b is the range of C.V., $b = 10.5$; $x_{\min}$ is the minimum BCL, $x_{\min} = 166$ (in ms); τ is the time constant of recovery of C.V., $\tau = 390$ (in milliseconds). Similar to tissue preparations, these engineered cardiac cell networks demonstrate a clear rate-dependence of conduction velocity, which might prove important in the genesis of arrhythmias when stimulated at higher frequencies.

E. Macroscopic Imaging of Intracellular Calcium

In Fig. 6, the CFI method in conjunction with LED illuminations was used for the first time to measure $[Ca^{2+}]_i$. The $[Ca^{2+}]_i$ traces (9-point median filter) are from a cell monolayer paced at

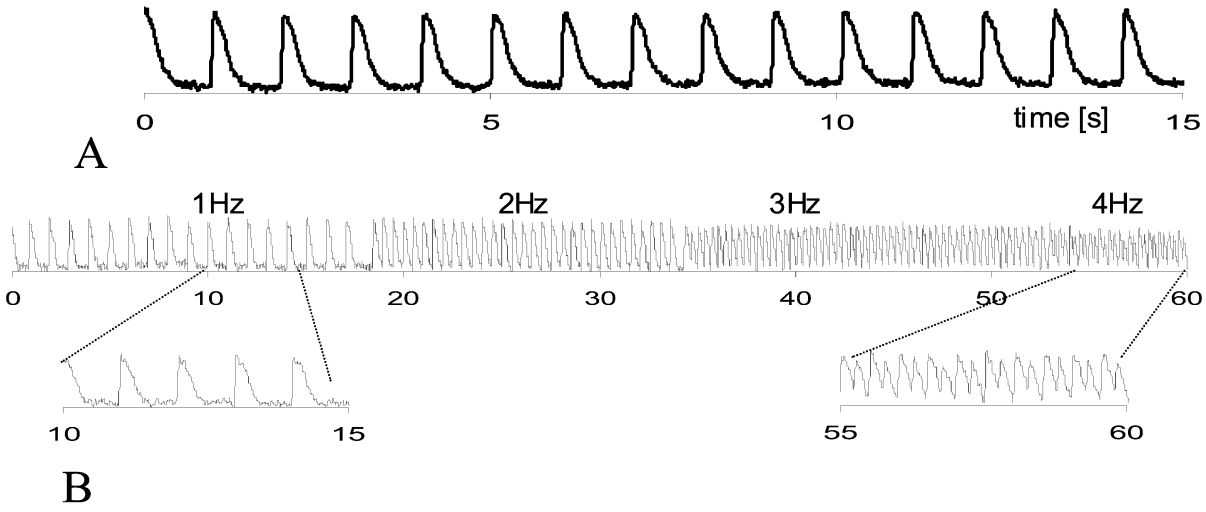

Fig. 7. Microscopic V_m fluorescence signals from a network of less than ten cells in response to epi-illumination with green LEDs; PMT was used as a detector. **A** Representative response to 1-Hz pacing. **B** One minute of recording in a different sample, demonstrating a very high stability to photobleaching. The frequency response over 1–4 Hz range is shown, with action potential alternans appearing at 4 Hz.

2 Hz. Blue LED illumination and an Acid Yellow emission filter was used. A single trace and multisite (ten- channel) recordings are shown in Fig. 6(a). Fig. 6(b) shows $[Ca^{2+}]_i$ recordings from another monolayer with LED illumination and a traditional QTH lamp (bandpass excitation filter (Chroma) 480 ± 15 nm) at the same spatial location. The morphology of the calcium transients was very similar under the two illumination approaches. Time to peak was 60–70 ms, and the duration of the calcium transients (from the time of 50% rise to 50% recovery) was about 150 ms for 2-Hz pacing rate. These data compare well with microscopic measurements in our lab at $10\times$ and $20\times$ using Fluo-3 or Fura-2 as the fluorophore.

F. Microscopic Imaging of Transmembrane Potentials

Finally, we tested the ability of the 3 LED module to serve as an (epi-illumination) excitation light source in a microscopic setting. The recording field of view was aperture-limited to less than ten cells, the emitted fluorescence from which was collected with a PMT in a photon-counting mode. Fig. 7(a) shows a representative trace of paced (1 Hz) action potentials. Fig. 7(b) from another sample demonstrates 1) the excellent stability of the signal over time – virtually no photobleaching within 1 min of recording at the same location; and 2) the frequency response of the cells in the interval 1–4 Hz. This particular sample was unable to respond 1:1 at high frequency, and V_m alternans are visible at 4 Hz.

Figs. 4–7 demonstrate that the optical recordings with only three LEDs are clear enough to provide data concerning the durations of action potentials and calcium transients, as well as activation maps of wave propagation. The signal-to-noise ratio (SNR), averaged over all the mapped sites, was 3.8 for the experiment in Fig. 4(a) and (b). The SNR was calculated from the raw traces as the ratio of signal amplitude to the peak-to-peak noise extracted from the periods of rest between the action potentials. Moreover, the minimal (three LEDs) illumination module was able to serve as an epi-illumination light source for microscopic measurements of transmembrane potentials. This is impressive, given the high optical power requirements for microscope illumination in order to collect enough emitted photons from only a couple (< 10) of cells. Therefore, LED illumination seems a viable alternative for fluorescence measurements of electrical activity in cardiac myocytes in a wide range of applications at both the micro- and macroscopic scale, tracing temporal and spatial determinants of cardiac propagation and arrhythmogenesis.

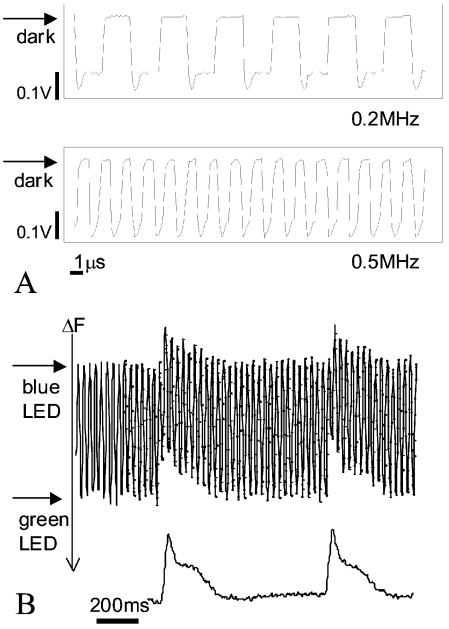

Fig. 8. Electronic light modulation of the LED output. **A** The optical output of the green LED illumination module in response to rectangular pulses at 0.2 and 0.5 MHz. The signal was recorded at 5 MHz sampling rate. **B** Fluorescence measurements of transmembrane potentials with modulated light (switching between green and blue LEDs with 0.9 KHz) and continuous green light. Sampling rate was 1 KHz. Even at this low modulation rate, the envelope of the signal is clearly visible at both light levels.

G. Light Modulation

Unlike conventional excitation light sources, the LEDs are unique in allowing for easy electronic light modulation at a high frequency. We illustrate this ability in Fig. 8. The optical output

of our green LED illumination module was electronically gated with rectangular pulses at 0.2 and 0.5 MHz. Higher frequencies were achieved but not digitally recorded due to the limitation of our data acquisition board, which had a maximum sampling rate of 5 MHz. Since the LED module switching speed was of interest in this experiment, measurements in Fig. 8(a) were conducted with a fast trans-impedance amplifier (AD8015) with a low feedback resistor, different from the amplifier settings in our original measurement system. Furthermore, in Fig. 8(b) fluorescence measurements of transmembrane potentials were obtained (with our measurement system) with excitation light from two LED modules that were gated alternately to provide a dual excitation light frequency. The illumination module was switched between green and blue LEDs at 0.9 kHz; acquisition rate was 1 kHz. Even at this low modulation rate, the envelope of the signal was clearly visible at both light levels, and is similar to that obtained at the same site with continuous illumination.

IV. Discussion and Conclusion

We present fluorescence measurements of electrical activity in cardiac cell networks at the micro-and macro- scale using an all-solid-state system. The system incorporates two simple, cost-effective solutions for excitation light sources and emission wavelength selection.

The LEDs used as light sources offer not only great cost reduction, but also portability, low-voltage operation, easy handling and control. Moreover, battery operation offers additional signal stability. Our assessment of baseline changes in up to 10 min continuous measurements confirmed that the LEDs are stable light sources, in fact superior to a QTH lamp with a good power supply. Additionally, in terms of long-term stability, the guaranteed steady-state lifetime of the Nichia LEDs is > 1000 h, the steady-state lifetime of a 250-W QTH lamp greatly depends on the driving voltage and is typically between 50–200 h. The SNRs observed in the voltage traces for the LED and QTH illumination were comparable, but a direct conclusion about relative SNR is not straightforward for several reasons. First, it is not trivial to compare recordings from two different light sources, since the radiant pattern of illumination can differ significantly between the two. The QTH light was passed through a fiber-optic bundle, which emits a cone of light, while the LED has a less uniform and more centrally focused beam pattern. Therefore, we found that minor adjustments in the LED position had a great effect on SNR. Higher SNRs for the LED illumination could be obtained than those shown, but it is difficult to determine which should be considered representative. Additionally, the noise in the recordings is due not only to illuminator noise, but also to shot noise of the light signal and the dark noise of the photodetector, which may have dominated the measurements in our particular system.

Other LED advantages over traditional light sources that are important for measurements in live cells include the elimination of ultraviolet and infrared radiation, both of which comprise the major portion of the output of the lamps currently in use, and require additional filters to remove. Various future applications could be enabled by the LED use, that are not feasible with the current illumination sources. For example, the development of genetic GFP-conjugated voltage/calcium-sensitive probes [23], [24], allowing *in vivo* expression, might allow fluorescence measurements of $\mathrm{V_m}$ and $\mathrm{Ca^{2+}}$ during cell culture in the incubator with portable stand-alone units. In such situations, only a miniature LED-based illumination would be adequate and CFI, using fiber optics and no relay lenses, is well suited for such an application.

Probably the most attractive attribute of the LEDs as excitation light sources is the easy electronic modulation of their light output, which could be combined with synchronous detection (with a lock-in amplifier, for example) to improve the SNR. By modulating the excitation light at a known frequency, the signal of interest is shifted from (dc-100 Hz) frequencies up to an amplitude-modulated carrier frequency. This allows improvement of SNR because amplifiers typically have 1/f noise (higher noise at lower frequencies).

The ability to modulate light might offer an elegant way of performing excitation-ratiometric measurements with high temporal resolution, as have been obtained with calcium (Fura-2) or voltage-sensitive ANEPPS dyes [25], or combined calcium and voltage experiments. Note that mechanical light choppers and filter wheels typically operate at 30–50 Hz [20], reaching 1 kHz only in expensive state-of-the-art products, while an LED-based illumination module and the fast calcium- and voltage- sensitive dyes allow for electrically gated excitation light at much higher frequencies. For example, the ratiometric calcium dye Fura-2 exhibits a considerable excitation spectrum shift, and is a good candidate for LED experiments (switching between 340 nm and 380 nm). However, the currently available ultrabright UV LEDs can cover only one of the required wavelengths (380 nm); 340 nm LEDs are still in the research stage. Previous experiments in lipid vesicles have suggested the possibility to perform excitation ratiometry with di-8-ANEPPS using 440 nm and 535 nm [26]. Since the behavior of these fluorescent probes is dependent on the particular environment, we scanned a series of excitation wavelengths (365, 380, 450, 480, 535 nm) to determine if the recorded fluorescence signals in cardiac cell monolayers stained with di-8-ANEPPS could be used for constructing such a ratio under modulated LED illumination. A significant decrease in intensity (and SNR) of the acquired fluorescence for wavelengths lower than 535 nm was observed. This intensity change appeared to obscure the small excitation spectrum shift, and to mask the expected polarity change in the obtained fluorescence signals, as also suggested by previous studies [26], [27]. Based on these results, the difficulty in measuring useful excitation ratio with di-8-ANEPPS should be recognized. In summary, experimental design involving light modulation is an attractive LED application, but imposes stringent requirements for choosing the proper filters (both excitation and emission) and detectors to equalize intensity levels at the two wavelengths and to guarantee fast response and proper sensitivity.

Compared to tissue preparations and whole heart, the cell monolayers used here impose more stringent sensitivity requirements for optical measurements. Based on data from Knisley [28], Girouard *et al.* [5], and Baxter [29] for the excitation and emission light distribution in the tissue depth, the fluorescent signals from a single layer of cells (thickness 10–20 μm) are 20–100 times lower than those from a tissue preparation with

multiple contributing cell layers. Thus, there is no foreseeable obstacle for the application of these versatile semiconductor light sources in cardiac optical mapping studies in general. Indeed, a recent report presented the use of high-power blue LEDs in a single channel optical probe for V_m in a Langendorff preparation [30].

The simple and inexpensive methods for preparing custom-designed emission filters, as presented here, offer flexibility in choosing the desired filter properties such as spectral characteristics. However, for CFI applications, thinness of the filter must be traded off against filter absorption. Additionally, identifying the proper dyes for the filters, in terms of absorption spectrum, solubility and lack of auto-fluorescence, could be very time-consuming. Albeit low-cost and flexible, the plastic filters, described here and needed for CFI, might not be the best choice for general optical applications.

Optical mapping in engineered cardiac cell constructs opens the door to studies of clinically important phenomena related to cardiac excitation such as the induction, evolution and termination of reentrant waves, which depend on tissue properties such as the rate-dependence of conduction velocity. This paper offers novel, inexpensive tools for explorations in this area, allowing measurements at the macro-and micro- scale.

ACKNOWLEDGMENT

The authors would like to thank A. Sathye for help with the stability assessment tests.

REFERENCES

[1] I. R. Efimov, M. Biermann, and D. Zipes, "Fast fluorescent mapping of electrical activity in the heart: Practical guide to experimental design and applications," in *Cardiac Mapping*, M. Shenasa, M. Borggrese, and G. Breithardt, Eds. London, U.K.: Blackwell, 2003.

[2] G. Salama, "Optical measurements of transmembrane potential in heart," in *Spectroscopic Membrane Probes*, L. M. Loew, Ed. Boca Raton, FL: CRC, 1988, pp. 137–199.

[3] S. M. Dillon, "Optical recordings in the rabbit heart show that defibrillation strength shocks prolong the duration of depolarization and the refractory period," *Circ. Res.*, vol. 69, pp. 842–856, 1991.

[4] I. R. Efimov, Y. Cheng, M. Biermann, D. V. Wagoner, T. Mazgalev, and P. Tchou, "Transmembrane voltage changes produced by real and virtual electrodes during monophasic defibrillation shock delivered by an implantable electrode," *J. Cardiovasc. Electrophysiol.*, vol. 8, pp. 1031–1045, 1997.

[5] S. D. Girouard, K. Laurita, and D. Rosenbaum, "Unique properties of cardiac action potentials recorded with voltage-sensitive dyes," *J. Cardiovasc. Electrophysiol.*, vol. 7, pp. 1024–1038, 1996.

[6] R. A. Gray, J. Jalife, A. Panfilov, W. Baxter, C. Cabo, J. Davidenko, and A. Pertsov, "Mechanisms of cardiac fibrillation," *Science*, vol. 270, pp. 1222–1225, 1995.

[7] J. P. Wikswo, S. F. Lin, and R. A. Abbas, "Virtual electrodes in cardiac tissue: A common mechanism for anodal and cathodal stimulation," *Biophys. J.*, vol. 69, pp. 2195–2210, 1995.

[8] S. Rohr, D. Shoelly, and A. G. Kleber, "Patterned growth of neonatal rat heart cells in culture. Morphological and electrophysiological characteristics," *Circ. Res.*, vol. 68, pp. 114–130, 1991.

[9] V. G. Fast and R. E. Ideker, "Simultaneous optical mapping of transmembrane potential and intracellular calcium in myocyte cultures," *J. Cardiovasc. Electrophysiol.*, vol. 11, no. 5, pp. 547–556, 2000.

[10] S. Rohr and J. P. Kucera, "Optical recording system based on a fiber optic image conduit: Assessment of microscopic activation patterns in cardiac tissue," *Biophys. J.*, vol. 75, pp. 1062–1075, 1998.

[11] L. Tung and A. G. Kleber, "Virtual sources associated with linear and curved strands of cardiac cells," *Amer. J. Physiol. Heart Circ. Physiol.*, vol. 279, no. 4, pp. 1579–1590, 2000.

[12] P. Schaffer, H. Ahammer, W. Mueller, B. Koidl, and H. Windisch, "Di-4-ANEPPS causes photodynamic damage to isolated cardiomyocytes," *Pflueg Arch. Euro. J. Physiol.*, vol. 331, pp. 548–551, 1994.

[13] G. Bub, L. Glass, N. Publicover, and A. Shrier, "Bursting calcium rotors in cultured cardiac myocyte monolayers," in *Proc. Nat. Acad. Sci. USA*, vol. 95, 1998, pp. 10283–10 287.

[14] E. Entcheva, S. N. Lu, R. H. Troppman, V. Sharma, and L. Tung, "Contact fluorescence imaging of reentry in monolayers of cultured neonatal rat ventricular myocytes," *J. Cardiovasc. Electrophysiol.*, vol. 11, no. 6, pp. 665–676, 2000.

[15] J. Y. Wu and L. B. Cohen, "Optical measurement of membrane potential," in *Fluorescent and Luminescent Probes for Biological Activity: A Practical Guide to Technology for Quantitative Real-Time Analysis*, W. T. Mason, Ed. San Diego, CA: Academic, 1999, pp. 389–404.

[16] L. M. Loew, "Voltage-sensitive dyes: Measurement of membrane potentials induced by DC and AC electric fields," *Bioelectromagnetics*, vol. Suppl 1, pp. 179–189, 1992.

[17] E. Entcheva, "Novel approaches to imaging electrical activity in engineered cardiac cell constructs," *Ann. Biomed. Eng.*, vol. 29, no. 1, p. S46, 2001.

[18] L. Fiore, G. Corsini, and L. Geppetti, "Application of nonlinear filters based on the median filter to experimental and simulated multiunit neural recordings," *J. Neurosci. Meth.*, vol. 70, no. 2, pp. 177–184, 1996.

[19] J. R. Lackowicz, *Principles of Fluorescence Spectroscopy*. New York: Kluwer Academic/Plenum, 1999.

[20] A. Bullen and P. Saggau, "High-speed, random-access fluorescence microscopy: II. Fast quantitative measurements with voltage-sensitive dyes," *Biophys. J.*, vol. 76, no. 4, pp. 2272–2287, 1999.

[21] R. P. Haugland, *Handbook of Fluorescent Probes and Research Chemicals*. Eugene, OR: Molecular Probes Inc, 1996, pp. 511–587.

[22] D. A. Ryer, *Light Measurements Handbook*. Newburyport, MA: International Light, 1997.

[23] G. Guerrero, M. S. Siegel, B. Roska, E. Loots, and E. Y. Isacoff, "Tuning flash: Redesign of the dynamics, voltage range, and color of the genetically encoded optical sensor of membrane potential," *Biophys. J.*, vol. 83, no. 6, pp. 3607–3618, 2002.

[24] M. S. Siegel and E. Y. Isacoff, "A genetically encoded optical probe of membrane voltage," *Neuron*, vol. 19, no. 4, pp. 735–741, 1997.

[25] J. Zhang, R. M. Davidson, M. D. Wei, and L. M. Loew, "Membrane electric properties by combined patch clamp and fluorescence ratio imaging in single neurons," *Biophys. J.*, vol. 74, no. 1, pp. 48–53, 1998.

[26] V. Montana, D. L. Farkas, and L. M. Loew, "Dual-wavelength ratiometric fluorescence measurements of membrane potential," *Biochemistry*, vol. 28, no. 11, pp. 4536–4539, 1989.

[27] E. Gross, J. r. Bedlack_RS, and L. M. Loew, "Dual-wavelength ratiometric fluorescence measurement of the membrane dipole potential," *Biophys. J.*, vol. 67, no. 1, pp. 208–216, 1994.

[28] S. B. Knisley, "Transmembrane voltage changes during unipolar stimulation of rabbit ventricle," *Circ. Res.*, vol. 77, pp. 1229–1239, 1995.

[29] W. T. Baxter, S. F. Mironov, A. V. Zaitsev, J. Jalife, and A. M. Pertsov, "Visualizing excitation waves inside cardiac muscle using transillumination," *Biophys. J.*, vol. 80, no. 1, pp. 516–530, 2001.

[30] I. Kodama, I. Sakuma, N. Shibata, S. B. Knisley, R. Niwa, and H. Honjo, "Regional differences in arrhythmogenic aftereffects of high intensity DC stimulation in the ventricles," *Pacing Clin. Electrophysiol.*, vol. 23, no. 5, pp. 807–817, 2000.

Emilia Entcheva (S'96–M'98) received the B.S. and M.S. degrees in electrical engineering from the Technical University of Sofia, Sofia, Bulgaria, in 1988; and the Ph.D. degree in biomedical engineering from The University of Memphis, Memphis, TN, in 1998.

After a postdoctoral fellowship at The Johns Hopkins University, Baltimore, MD, in 2001 she became an Assistant Professor of Biomedical Engineering, Physiology and Biophysics at Stony Brook University, Stony Brook, NY. Her research interests include engineering functional cardiac tissue in the lab using microfabrication, elastic and biodegradable polymers; developing optical techniques and algorithms for the mapping of electrical and mechanical activity in the obtained tissue equivalents; and computer modeling in cardiac electrophysiology.

Yordan Kostov (M'00) received the B.S. and M.S. degrees in electrical engineering with honors from the Odessa Polytechnic Institute, former USSR, in 1987; and the Ph.D. degree in electrical and chemical engineering from the Bulgarian Academy of Sciences, Sofia, Bulgaria, in 1993. Then he was awarded a post-doctoral fellowship from the German Service for Academic Exchange, which he spent at the Institute for Technical Chemistry, University of Hannover, Hannover, Germany.

In 1994, he became an Assistant Professor in the Department of Biotechincs, Technical University of Sofia, Sofia, Bulgaria. Since 1999, he is with the University of Maryland Biotechnology Institute, and the Department of Chemical and Biochemical Engineering, University of Maryland, Baltimore County (UMBC), Baltimore, where he is currently a Research Assistant Professor. He is involved in the development of chemical and biochemical sensors for biomedical applications.

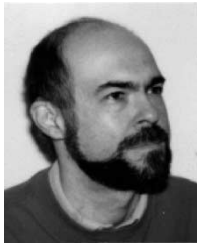

Elko Tchernev received the M.S. degree in electrical engineering from the Technical University of Sofia, Sofia, Bulgaria, in 1984, and the M.S. degree in computer science from The University of Memphis, Memphis, TN, in 1998. He is currently working towards the Ph.D. degree in computer science at The University of Maryland – Baltimore County, Baltimore. His research interests are in the area of genetic programming, evolutionary computation, neural networks, and computer architecture.

Leslie Tung (M'88) received the B.S., M.S., and Ph.D. degrees from the Massachusetts Institute of Technology, Cambridge, in 1972 and 1978, respectively, all in electrical engineering.

He was a Postdoctoral Fellow at the Department of Physiology at the University of Pennsylvania, Philadelphia, and joined the faculty there as Research Assistant Professor. Since 1986, he has been with the Department of Biomedical Engineering, the Johns Hopkins University, Baltimore, MD, where he is currently an Associate Professor and Head of the Cardiac Bioelectric Systems Laboratory. His research interests are in the electrophysiological properties of engineered networks of heart cells, as they relate to mechanisms underlying reentrant arrhythmias, electrical cardioversion and stimulation. He utilizes microfabrication techniques, tissue culture, optical mapping, theoretical analysis, and computational models to study the experimental and theoretical behavior of cardiac cell networks.